sylation of the serine/threonine residues from UDP-*N*-acetyl-D-galactosamine[32]. However, similar times are required for insertion into the endoplasmic reticulum membrane, glycosylation and appearance at the cell surface. Whether glycophorin A contains an additional NH_2-terminal signal sequence found in most glycoprotein precursors[33] is not known and is being investigated.

We thank Anneli Asikainen, Marja Wilkman and Liisa Alajoki for assistance. K562 cells were obtained from Dr K. Nilsson. This study was supported by the Academy of Finland, the Finnish Cancer Society and Lääke Oy.

Received 12 February; accepted 8 May 1979.

1. Bretscher, M. S. & Raff, M. C. *Nature* **258**, 43–49 (1975).
2. Gahmberg, C. G. in *Dynamic Aspects of Cell Surface Organization* (eds Poste, G. & Nicolson, G. L.) 371–421 (North-Holland, Amsterdam, 1977).
3. Bretscher, M. S. *Nature new Biol.* **231**, 229–232 (1971).
4. Bretscher, M. S. *J. molec. Biol.* **98**, 831–833 (1975).
5. Nicolson, G. L. & Singer, S. J. *J. Cell Biol.* **60**, 236–248 (1974).
6. Gahmberg, C. G. & Hakomori, S. J. *J. biol. Chem.* **248**, 4311–4317 (1973).
7. Steck, T. L. & Dawson, G. *J. biol. Chem.* **249**, 2135–2142 (1974).
8. Rothman, J. E. & Lodish, H. F. *Nature* **269**, 775–780 (1977).
9. Katz, F. N., Rothman, J. E., Knipe, D. M. & Lodish, H. F. *J. supramolec. Struct.* **7**, 353–370 (1977).
10. Garoff, H., Simons, K. & Dobberstein, B. *J. molec. Biol.* **124**, 587–600 (1978).
11. Rothman, J. E., Katz, F. N. & Lodish, H. F. *Cell* **15**, 1447–1454 (1978).
12. Li, E., Tabas, I. & Kornfeld, S. *J. biol. Chem.* **253**, 7762–7770 (1978).
13. Steck, T. L. *J. Cell Biol.* **62**, 1–19 (1974).
14. Marchesi, V. T., Furthmayr, H. & Tomita, M. *A. Rev. Biochem.* **45**, 667–698 (1976).
15. Marchesi, V. T., Tillack, T. W., Jackson, R. L., Segrest, J. P. & Scott, R. E. *Proc. natn. Acad. Sci. U.S.A.* **69**, 1445–1449 (1972).
16. Furthmayr, H. *Nature* **271**, 519–524 (1978).
17. Segrest, J. P., Jackson, R. L., Andrews, E. P. & Marchesi, V. T. *Biochem. biophys. Res. Commun.* **44**, 390–395 (1971).
18. Tomita, M. & Marchesi, V. T. *Proc. natn. Acad. Sci. U.S.A.* **72**, 2964–2968 (1975).
19. Tomita, M., Furthmayr, H. & Marchesi, V. T. *Biochemistry* **17**, 4756–4770 (1978).
20. Gahmberg, C. G., Jokinen, M. & Andersson, L. C. *Blood* **52**, 379–387 (1978).
21. Tanner, M. J. A. & Anstee, D. J. *Biochem. J.* **155**, 701–703 (1976).
22. Dahr. W., Uhlenbruck, G., Leikola, J., Wagstaff, W. & Landfield, K. *J. Immunogenet.* **3**, 329–346 (1976).
23. Gahmberg, C. G., Myllylä, G., Leikola, J., Pirkola, A. & Nordling, S. *J. biol. Chem.* **251**, 6108–6116 (1976).
24. Lozzio, C. B. & Lozzio, B. B. *Blood* **45**, 321–334 (1975).
25. Andersson, L. C., Nilsson, K. & Gahmberg, C. G. *Int. J. Cancer* **23**, 143–147 (1979).
26. Gahmberg, C. G., Jokinen, M. & Andersson, L. C. *J. biol. Chem.* (in the press).
27. Gahmberg, C. G. & Andersson, L. C. *J. biol. Chem.* **252**, 5888–5894 (1977).
28. Andersson, L. C., Jokinen, M. & Gahmberg, C. G. *Nature* **278**, 364–365 (1979).
29. Schachter, H. *et al. J. biol. Chem.* **245**, 1090–1100 (1970).
30. Steck, T. L. in *Membrane Research* (ed. Fox, C. F.) (Academic, New York, 1972).
31. Gahmberg, C. G. *J. biol. Chem.* **251**, 510–515 (1976).
32. McGuire, E. J. & Roseman, S. *J. biol. Chem.* **242**, 3745–3747 (1967).
33. Blobel, G. & Dobberstein, B. *J. Cell Biol.* **67**, 835–851, 852–867 (1975).
34. Laemmli, U. K. *Nature* **227**, 680–685 (1970).
35. Bonner, W. M. & Laskey, R. A. *Eur. J. Biochem.* **46**, 83–88 (1974).
36. Rice, R. H. & Means, G. E. *J. biol. Chem.* **246**, 831–832 (1971).
37. Gahmberg, C. G. & Andersson, L. C. *J. exp. Med.* **148**, 507–521 (1978).
38. Sage, J. H. & Green, R. W. *Meth. Enzym.* **28**, 332–339 (1972).

The three-dimensional structure of tubulin protofilaments

L. A. Amos & T. S. Baker*

MRC Laboratory of Molecular Biology, Cambridge, UK

A three-dimensional image of tubulin protofilaments, reconstructed to 20 Å resolution from electron micrographs of negatively stained zinc-induced sheets, has been used to generate an improved model for microtubule substructure. This model has been used to phase a reconstructed image from X-ray amplitudes, which is compatible with the electron microscope results.

THE three-dimensional structure of eukaryotic microtubules has been studied by electron microscopy (EM) of individual specimens[1–4] and by X-ray diffraction of oriented gels of microtubules[5–7]. Results from EM suggested an arrangement of monomer subunits on the same helical surface lattice for both neurotubules and flagellar microtubules[2,3]. Early X-ray diffraction patterns seemed to be in disagreement[5], but this was resolved after further studies[6,7]; the X-ray data now seem to be quite consistent with the geometry determined by EM. However, there still seem to be some differences in the data, especially with respect to the shapes of the subunits, even at very low (40 Å) resolution. Even different EM studies have tended to give somewhat different impressions of the substructure. In images of brain tubulin sheets, which are thought to be the equivalent of opened-out microtubules, each tubulin subunit seemed to be split longitudinally into two separate domains[2,4]. This feature was not detected in a three-dimensional analysis of intact flagellar microtubules[3], in which the monomers apparently consisted of single globular units, although the overall outline of the subunits was similar. Furthermore, a model based on an interpretation of the intensity distribution in X-ray diffraction patterns of brain microtubules[7] showed subunit shapes which were incompatible with either of the classes of image obtained by EM. We now present a new model of the structure of tubulin, based on three-dimensional EM image reconstruction of extended brain tubulin sheets, which seems to explain the differences between the earlier images and suggests a compatible interpretation of the X-ray diffraction patterns from microtubules.

* Present address: Rosenstiel Basic Medical Sciences Research Center, Brandeis University, Waltham, Massachusetts 02154.

Zinc-induced tubulin sheets

The specimens we studied were the large two-dimensional crystalline arrays of brain tubulin which assemble in the presence of zinc ions[8,9]. These sheets are apparently made up of the same linear arrays of subunits, or protofilaments, as 'normal' sheets, which are often found in samples of repolymerised microtubule protein and which have been proposed as precursors in microtubule assembly[2,10]. Whereas normal sheets are usually no more than 12 protofilaments wide, presumably because a sheet of 13 protofilaments closes to form a microtubule, zinc-induced sheets may be 100 or more protofilaments wide and are therefore much better for periodic structural analysis. Studies of their projected structure have shown that protofilaments are arranged with alternating polarity (see Fig. 1*a*), so that these arrays have $P2_1$ crystallographic symmetry[11,12] The arrangement is thus quite different from that in a microtubule or a normal sheet, where all the protofilaments have the same polarity. However, the individual protofilaments seem to be very similar, having the same 48–49 Å side-to-side spacing in both types of sheet. This common feature suggests that the rotational orientation of a protofilament about its axis is similar in both structures. By comparing the obliquity of the projected subunit shapes in Fig. 1*a* with those in computer-filtered EM images of normal tubulin sheets[2,4], we were also able to deduce that the protofilament images labelled I in Fig. 1 represent the view from the outside of a normal microtubule[11]

0028–0836/79/0279—0607$01.00

Figure 1*a* was derived from four highly selected low-dose EM images of negatively stained specimens and includes data to 16 Å resolution[11]. To obtain a three-dimensional image, this untilted projection was combined with 40 independent images of sheets tilted through angles of 21°, 35° or 51° about various axes[14]. The number of different orientations of the sheets was more than sufficient to provide homogeneous data to 20 Å resolution within the angular range covered by tilting up to 51°. The intensities of most of the reflections fell to noise level within this range. Additional data, corresponding to higher tilt angles, which could not easily be reached by tilting in the microscope, were obtained from images of negatively stained specimens embedded in plastic and sectioned normal to the sheets[13]. These data were to about 40 Å resolution; the complete set of data is therefore still not fully isotropic, so that density variations in the direction normal to the sheets are not quite as well resolved as those in the plane of the sheets. Full details of data collection and analysis are presented elsewhere[13].

Three-dimensional model of the sheets

The main features of the reconstructed three-dimensional density distribution are illustrated in Figs 1*b* and 2. Viewed down its long axis, each protofilament is roughly triangular in shape, with one corner of the triangle protruding from one side of the sheet. Thus, the two exposed surfaces of a protofilament are very different. In longitudinal view, one surface has the form of a longitudinal ridge and the other has a flat ladder-like appearance, with sloping bi-lobed rungs. If we are correct in assuming that the protofilament images labelled I in Fig. 1*a* represent the view from outside a microtubule, then the ridged surface must be on the outside, while the ladder-like appearance should occur on the inside surface. This is discussed in detail later.

The apparent thickness of the negatively stained sheets, as observed directly in section and also as estimated from the tilted views, is only about 45–50 Å, compared with a difference of 70–80 Å between the inner and outer radii of a microtubule, as estimated from X-ray diffraction measurements[5–7]. Therefore, the sheets have probably shrunk in this dimension as they dried down on to the EM support grid. It is also possible that part of the apparent reduction in thickness results from the masking of fine surface features extending into the negative stain, or by positive staining of protein on the protofilament surface. Thus, the ridge in particular may extend out further than it seems to in the reconstructed image. The importance of such effects is discussed later.

As described previously[11], each protofilament clearly consists of an alternating linear array of two kinds of slightly different subunits, believed to represent the two species of 55,000 molecular weight monomer which form the tubulin heterodimer[15]. Both kinds of subunit appear in projection as elongated shapes (Fig. 1*a*), with their long axes at about 40° to the protofilament axes. If one attempts to follow the density corresponding to an individual subunit through successive sections parallel to the central plane of the sheet (Fig. 2), the peaks move gradually downwards between the first and last sections. The subunits thus apparently have the general form of tilted ellipsoids when viewed from the side, as well as face on.

The difference between the two kinds of subunit seems to be rather less in three dimensions than in the two-dimensional projection, showing significantly only at the ladder-like inside surface of the protofilaments. The apparently more definite division into two domains of one of the two subunits presumably represents a real difference in the internal structure of the two monomers.

The pattern of interprotofilament contacts is also not as complex as suggested by the original projection (Fig. 1*a*), where the contacts between each pair of subunits seem to be represented by two separate regions of higher density in the interprotofilament gap[11]. In the three-dimensional model, the contacts seem to take place over single fairly broad zones (Fig. 2, P to Q or R to S), centred on the central plane of the sheets. The complexity in projection is due to superposition of the intricate stain distributions at the two surfaces of the sheets.

Model protofilaments rearranged to represent a microtubule

Normal microtubules observed *in situ* consist, in most cells, of 13 longitudinal protofilaments[16] in a polar arrangement[3]. Reassembled microtubules often contain 14 protofilaments[17], but these are probably aberrant structures. To simulate a normal

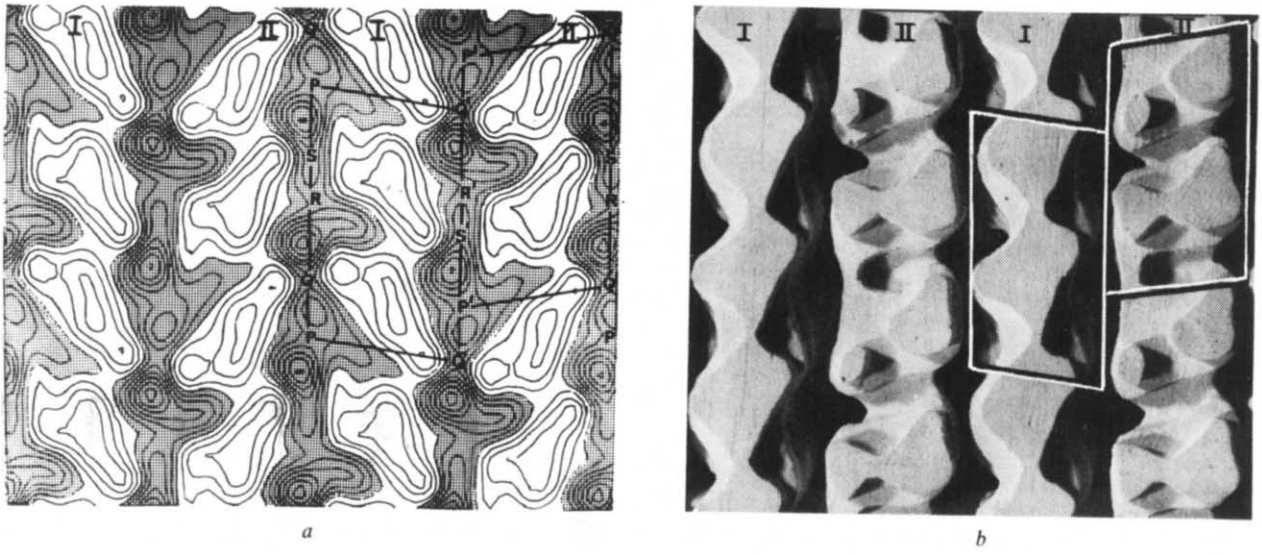

a *b*

Fig. 1 *a*, Computer reconstructed image of negatively stained zinc–tubulin sheets seen in projection[11]. The variation in density is represented by evenly spaced contour levels. Regions dominated by negative stain are shown shaded while absence of stain, corresponding to protein, is white. Neighbouring longitudinal protofilaments, each 48 Å wide, are related by $P2_1$ symmetry, about screw dyad axes normal to the protofilaments and in the plane of the sheet. Each globular unit along a protofilament is thought to represent a monomer of α- or β-tubulin. The boxes drawn on the image each enclose what seems to be an 80 Å long α–β heterodimer. *b*, A solid model of part of a zinc–tubulin sheet, with boundaries which follow one of the contour levels in Fig. 2. Two different surfaces of the protofilaments are presented, as adjacent protofilaments face different ways.

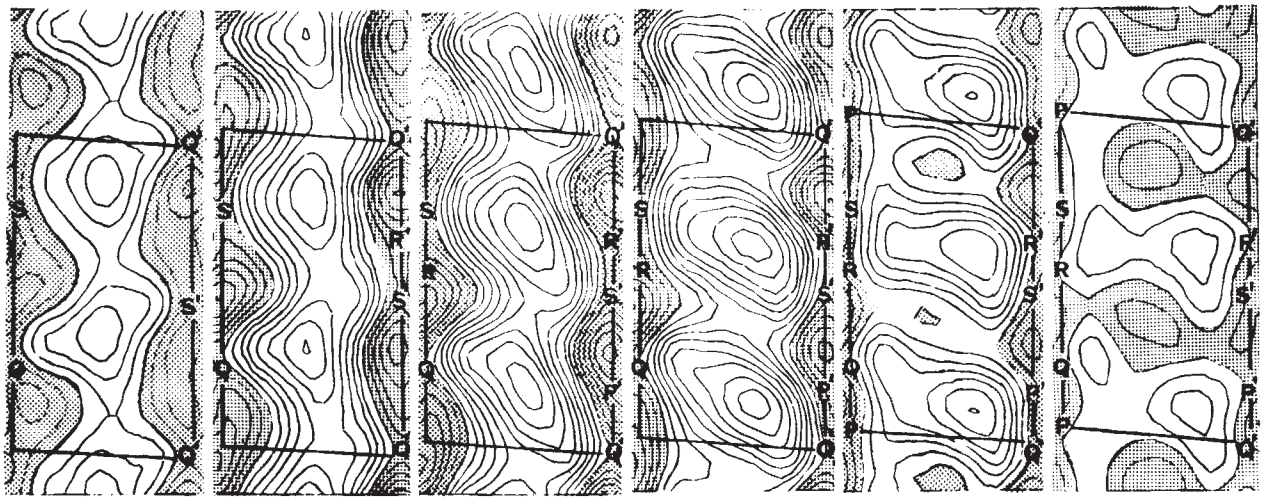

Fig. 2 Sections at different levels (z) through one protofilament of the reconstructed three-dimensional model of the negatively stained zinc–tubulin sheets. Below each section is given its distance from the plane through the centre of the sheet. Features at the boundaries of the protofilament are labelled as in the projection in Fig. 1*a*.

microtubule, therefore, we have arranged 13 model zinc–tubulin protofilaments, as shown in Fig. 3. In this arrangement, the former regions of contact between subunits in the sheet seem to match up again in the tubule, although in different polar orientations[11]. Probably the same hydrophobic regions of each subunit are involved in the assembly of both types of structure. The model in Fig. 3 was assembled with the ridged sides of the protofilaments outermost, so that the projected subunit shapes would agree with images of negatively stained normal sheets[2,4]. There are several observations which support this choice of orientation. One is the good agreement between the appearance of this model and that of the three-dimensional model reconstructed from images of intact flagellar microtubules[3]. In particular, the deep interprotofilament grooves are features of the outer surfaces of both models. The presence of these grooves at high radius is also stongly indicated by X-ray diffraction data[5–7]. If the wedge-shaped protofilaments were oriented with the ridged surface inwards, grooves would not be formed specifically at the outer surface; the interprotofilament contrast would be weaker and roughly equal at all radii between 70 and 150 Å. Clear images of sectioned normal microtubules[17,18] also support the conclusion that the protofilaments should appear in cross-section as outwardly pointing wedge shapes. A final observation which indicates that, in a normal microtubule, interprotofilament contact is limited to inner radii (less than 110 Å) is that the spacing of protofilaments in flat sheets (normal or zinc-induced) is consistently less (48–49 Å) than the spacing of 53 Å at the mean radius (110 Å) of a microtubule.

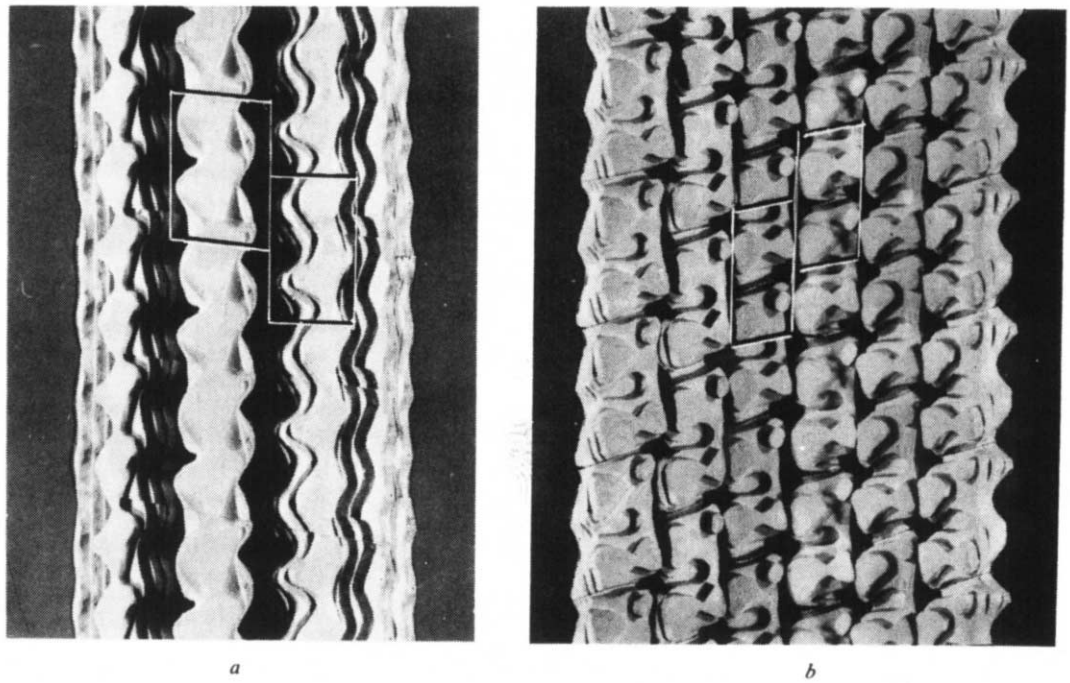

Fig. 3 *a*, Models of zinc-tubulin protofilaments from the reconstructed image shown in Fig. 1*b*, rearranged to conform to the helical symmetry established for a normal microtubule. Thus, the monomer subunits lie on a family of three shallow left-handed helices. The relative arrangement of tubulin dimers is that observed in complete flagellar microtubules[3] (see text). Two unit cells, each enclosing an 80-Å long α–β dimer, are outlined. *b*, Inside surface of part of a microtubule, opened out to form a 'normal' sheet. The polar arrangement of the protofilaments is the same as in *a*. Comparison of these images with the reconstructed three-dimensional model of intact flagellar microtubules[3], suggests that the bottom of the model, as shown in these two views, corresponds to the basal end of a flagellar microtubule.

The other assumption incorporated in the model shown in Fig. 3 is that the subunit dimers in adjacent protofilaments are in a staggered arrangement, as observed in complete flagellar microtubules, that is, the A-tubules of outer doublet microtubules[3] and the central singlet microtubules[1]. This is in fact the only helically symmetrical arrangement possible for a 13-protofilament microtubule in which the monomer subunits are arranged as shown. There is some evidence[7,12] that brain tubulin may sometimes reassemble *in vitro* in an alternative arrangement similar to that in a flagellar B-tubule[3], but when microtubules are reassembled from brain extracts containing a full complement of so-called microtubule associated proteins, the latter, seen as projections from the outsides of the tubules, seem to follow the symmetry of the A-tubule lattice[19]. This point is discussed in more detail elsewhere[20].

Variations in EM images

It is now understandable why somewhat variable images have been obtained in previous EM studies of protofilament structure. The appearance seems to vary according to which of the two different protofilament surfaces is the more strongly emphasised by the negative stain. The bi-lobed, or ladder-like appearance obtained for opened-out brain microtubules[2,3] corresponds rather closely to the appearance of the inner surface of the present model. Erickson[2] noted that the normal sheets, being curved in solution, always fell with the outer surface next to the carbon substrate of the EM grid. Presumably the inside surface, which was thereby most exposed to the negative stain subsequently applied to the grid, was more strongly contrasted than the outer surface. The outer surface of the three-dimensional image reconstructed from images of intact flagellar microtubules[3], on the other hand, closely resembles the outer surfaces of the protofilaments in the present model, whereas the inner surface showed much less detail. In the case of an intact microtubule, it seems that the outside is most strongly contrasted by negative stain. In the zinc-induced sheets the orientation of the protofilaments alternates. Differential staining of the two sides of such sheets probably explains the great difference in projection of adjacent protofilaments observed initially by Crepeau *et al.*[4]. However, the images we have used all show very good $P2_1$ symmetry[11], so we deduce that in our specimens each protofilament must be more or less equally well contrasted on both sides. The three-dimensional image reconstructed from

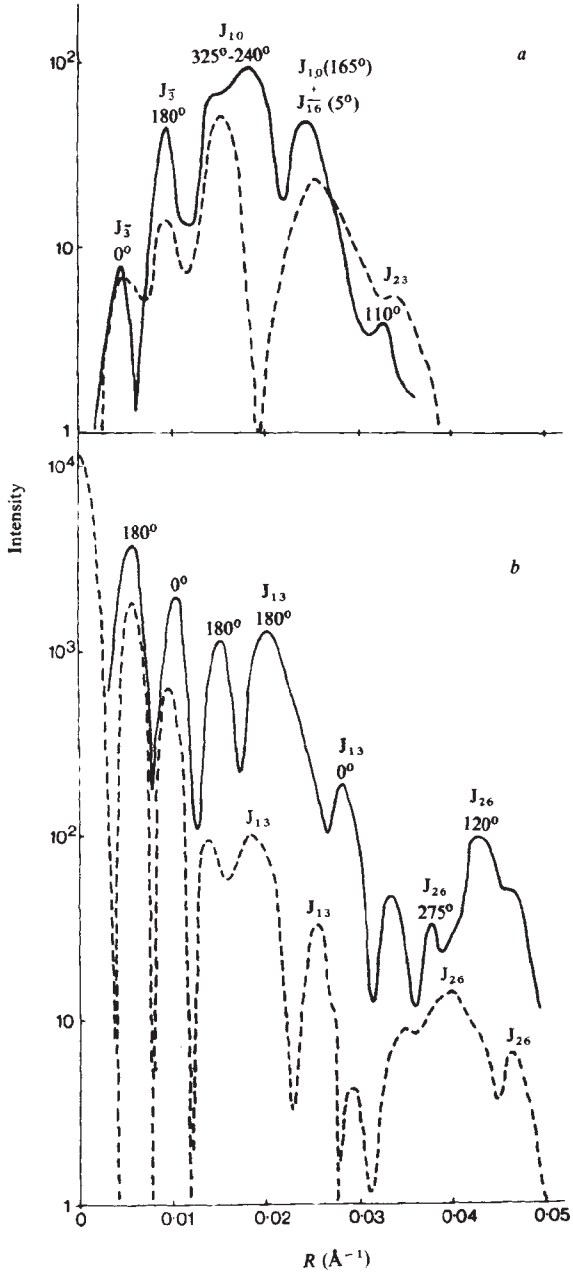

Fig. 4 Intensity distributions for the equatorial (*b*) and 40 Å (*a*) layer lines of diffraction patterns from real and model microtubules. The dashed lines represent the intensity distributions measured by Mandelkow *et al.*[7] in X-ray diffraction patterns obtained from oriented hydrated gels of microtubules. The solid lines follow cylindrically averaged intensity distributions calculated for a model microtubule, consisting of 13 zinc–tubulin protofilament images arranged on a mean radius of 110 Å; the density distributions were uniformly 'stretched' by 30% in the direction normal to the zinc–tubulin sheets, to correspond more closely to the microtubule dimensions estimated from X-ray diffraction data[7] (see text). The only significant effect of this is a slight change in the radial positions of the intensity peaks in the calculated diffraction pattern. The relative phases (for protein represented as positive density) determined for the various helical contributions are indicated above the intensity peaks. On the calculated equator, the strong peaks near the origin represent the transform of a hollow cylinder. The peaks at 0.020 $Å^{-1}$ and 0.028 $Å^{-1}$ (labelled J_{13}) arise mainly from the division of the cylinder into 13 distinct longitudinal protofilaments: the first is from 13-fold contrast at the outside of the cylinder, the second from the much weaker contrast on the inside. Second order diffraction from the protofilaments provides the main contributions to the last group of peaks (J_{26}): the weak inner peak of this group corresponds to features of the outside of the cylinder, the stronger peak to the inner side. On the 40 Å or second layer line (based on an axial repeat of 80 Å) of the calculated diffraction pattern, the two (J_3) peaks close to the meridian arise from outer and inner radii contributions from the family of three shallow left-handed helices; the apparently double third peak (J_{10}) (with varying phase across it) consists mainly of contributions from the 10 steeper, right handed helices at outer radii. The broad fourth peak includes a small contribution from the latter family at inner radius, but also significant contributions from the left-handed 16-member family at radii centred on a mean of about 110 Å. The calculated curves do not correspond exactly with those measured from X-ray diffraction patterns; for example, the relative intensities on the equator fall off differently and the J_{10} peak on the 40 Å layer line has a different shape. However, some differences are to be expected, as the model was derived by studying dehydrated protein embedded in metal stain, whereas the X-ray diffraction pattern is from hydrated unstained specimens and provides information about the contrast between protein and aqueous solvent.

them should therefore provide a more reliable impression of the structure than has been obtained from previous EM studies of tubulin structure.

However, because of artefacts due to dehydration, radiation damage and the limitations of negative stain contrast, the results obtained by EM are not wholly satisfactory for studying the native structure of proteins. Low-dose electron microscopy of unstained specimens, embedded in glucose or sucrose solutions to alleviate the effects of dehydration, has proved successful in studies of the substructure of certain thin two-dimensional crystals of biological origin[14,21]. However, the results obtained so far with tubulin sheets[4] have not been very promising, the resolution attained being somewhat less than that obtained from negatively stained specimens. The zinc–tubulin sheets, although they grow much larger than normal tubulin sheets, probably still do not allow sufficient averaging to compensate for the extremely low signal-to-noise ratio in EM images of unstained protein.

Diffraction patterns from microtubules

X-ray diffraction of oriented gels of hydrated microtubules provides information about the protein in its native state, but the X-ray patterns from native specimens do not provide sufficient data by themselves for the reconstruction of a three-dimensional image of the structure. One way of trying to supply the missing information at low resolution is to use phase information obtained by electron microscopy[7]. For this purpose, we have calculated a three-dimensional diffraction pattern for the model density distribution shown in Fig. 3. The calculated diffracted intensity distributions, averaged around the vertical axis to simulate diffraction from an oriented gel of microtubules, are shown in Fig. 4 for the equatorial and 40 Å layer lines, together with the corresponding relative intensities measured from X-ray diffraction patterns. These curves calculated for the rearranged zinc-tubulin protofilaments are surprisingly more similar to the X-ray curves than are the distributions obtained directly from optical diffraction patterns of negatively stained microtubules[1–4,7]. In the latter case, the peak closest to the meridian on the 40 Å layer line is usually the strongest on that layer line, a peak corresponding to the third peak on the X-ray 40 Å layer line is much weaker in the microtubule optical diffraction patterns and the other two X-ray peaks are absent. As discussed above, this seems to be because negative stain does not map out the surface of a protofilament in an intact microtuble as closely as it does that of a protofilament in a zinc–tubulin sheet.

Interpreting the X-ray patterns

Cohen *et al.*[6,7] have interpreted the low angle X-ray intensity distribution (Fig. 4, dashed lines) in terms of diffraction mainly from the inner and outer surfaces of the microtubules, which apparently have inner and outer radii of 70 and 150 Å respectively. The strong equatorial J_{13} and J_{26} reflections have both been identified as coming from the outer surface, with mean radii of 126 and 115 Å respectively. The series of four peaks on the 40 Å layer line were indexed as two J_{-3} contributions from outer and inner mean radii of 130 and 70 Å, followed by two J_{10} contributions from outer and inner mean radii of 120 and 70 Å.

Mandelkow *et al.*[7] attempted to reconstruct a three-dimensional model of a microtubule from the measured X-ray intensities, interpreted in the above manner, by combining them with phases determined by Erickson[2], and confirmed by their own observations, from two-dimensional EM images of microtubules opened out as sheets. (In calculated diffraction patterns from digitised images, with a phase origin equivalent to that used in Fig. 4, phases of 180° are found for each of the lattice points corresponding to single J_{13}, J_{26}, J_{-3} and J_{10} contributions.) However, as the relative intensities in the X-ray diffraction pattern and the diffraction patterns from the original EM images were very different, the hybrid reconstructed image[7] was also quite different from the original images, with elongated subunits sloping in the opposite direction. Without reasonable agreement between the two techniques, there is no justification for combining EM phases with X-ray amplitudes. It is now possible, however, from our analysis of the zinc–tubulin structure, to suggest some modifications to the above interpretation and phasing of the X-ray patterns, which lead to a much closer consistency between the X-ray and EM data.

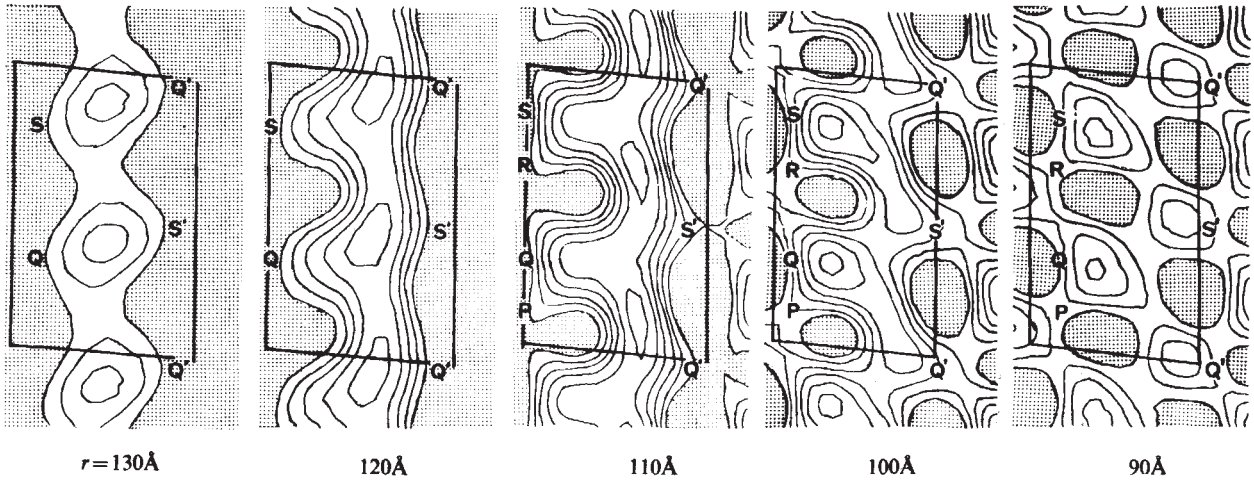

Fig. 5 Sections at different radii (r) through part of the reconstructed density distribution, calculated using Fourier amplitudes deduced from X-ray diffraction patterns of intact brain microtubules and phases (see Fig. 4) derived from model zinc–tubulin protofilaments rearranged as shown in Fig. 3. Features of the protofilament outline, which seem to correspond to those in the sections through the original image (Fig. 2), are labelled P to S. The two images are rather different at smaller radii; the sloping regions of high density (S to S′) and (Q to Q′) have a steeper slope than the corresponding regions in Fig. 2. (This difference seems to be less for one type of subunit in Fig. 2 than for the other.) As well as the equatorial and second (40 Å) layer lines shown in Fig. 4, the data included weak contributions from the third and fourth layer lines, estimated from the published X-ray patterns[7]. (Note that the indexing of the odd layer lines is determined by the arrangement of 80 Å long tubulin dimers, which is discussed below Fig. 3.) On the third layer line, an apparent J_2 contribution to the X-ray diffraction patterns was included with a phase of 45° but being weak has very little effect. The fourth layer line data consisted of approximately equal J_{-6} and J_7 contributions with phases of 210° and 50°, based on the model calculations.

The main difference from the previous interpretation is the source of the fourth peak from the meridian on the 40 Å layer line. Calculations from our model suggest it is probably a mixture of different contributions. As well as a small J_{10} contribution, it is likely to include a major J_{-16} contribution, with a mean radius of about 110 Å. It is not completely clear why a J_{-16} contribution is never observed in optical diffraction patterns from negatively stained microtubules or normal tubulin sheets, but it is probably for the same reason that the J_{10} contribution is weaker than the J_{-3} contribution, instead of stronger as in the X-ray patterns. The J_{-3} reflections clearly do come from the innermost and outermost surfaces of the structure and must be relatively easily revealed by negative stain, provided the surface in question is exposed to it. On the other hand, according to the present interpretation of the X-ray data, both the major J_{10} and J_{-16} contributions come from radii near the middle of the protein layer, into which it is presumably more difficult for the stain to penetrate. It may be relevant in this context that the X-ray diffraction patterns from dehydrated microtubules are said to be more similar to the optical diffraction patterns from electron micrographs[5,6]. This suggests that dehydration may cause the cleft between protofilaments to close up at inner radii and prevent features at these radii from contributing to the diffraction patterns.

Phasing the X-ray data

The relative phases we assign to the various contributions (Fig. 4), which were derived from the model shown in Fig. 3, also differ from those used by Mandelkow *et al.*[7]. This is mainly because, in the images of the flat sheets which supplied their phases, contributions from different radii in the microtubules become superimposed in projection. Unless features at all radii have corresponding spatial frequencies exactly in phase, the relative phases in the transform of such a flattened sheet will not agree with a separated set of either inside or outside surface contributions.

One significant difference is in the values assigned to the equatorial J_{26} intensity peaks. In EM images, the feature giving rise to the strongest diffraction contribution of this order is the shallow longitudinal groove bisecting one surface of each protofilament. We interpret this surface as being on the inside of a microtubule. In the X-ray diffraction patterns, the strongest J_{26} contribution seems to come from a radius of about 115 Å, which is within the extent of the deep interprotofilament grooves on the outside surface of the microtubule. Mandelkow *et al.*[7] originally related this contribution to the apparent splitting of the protofilaments (hence the 180° relative phase they assigned to it), but we now interpret it as most likely due to the sharpness of the ridges on the outer surfaces of the protofilaments. A smaller peak further out on the equator, at $R = 0.047$ Å^{-1}, probably arises from the apparent splitting of the protofilaments at inner radii.

According to this interpretation, the relative intensities of the two J_{26} contributions, from the inner and outer surfaces of the microtubules, are reversed in the X-ray diffraction patterns and the patterns calculated from the rearranged zinc–tubulin model. This could be due to artefacts of negative staining whereby the tips of the ridges on the outer surface of each protofilament might be swamped by negative stain and the outer surface J_{26} contribution thus reduced, while the shallow groove down the centre of the inside surface of the protofilament would tend to be over-emphasised by the stain, causing the inner surface J_{26} contribution to be enhanced.

Model from combined X-ray and EM data

A test of the above interpretation of the X-ray patterns is to see whether a reconstructed image, based on the X-ray amplitudes and the phases derived from the rearranged model, resembles the results from EM alone. Figure 5 shows sections through one protofilament of such a calculated microtubule density distribution. This structure can be compared with the zinc–tubulin image shown in Fig. 2, bearing in mind that the latter structure seems to have shrunk by 30–40% in the z-direction. There are some other differences between the two structures, as expected from the differences in the two sets of diffraction curves in Fig. 4. The sections in the region of the outside surface (around $z = 12$, 6 Å in Fig. 2; around $r = 130$, 120 Å in Fig. 5) are reasonably similar, but at inner radii there are some distinct differences. In particular, the 'rungs of the ladder' (around $z = -18$, -12 Å in Fig. 2; around $r = 90$, 100 Å in Fig. 5) seem much more steeply tilted, because of the greater strength of the J_{-16} contribution to the data, relative to the J_{-3} contribution. Also, the differences between the two species of tubulin subunit are much less obvious, because of the relative weakness of the third (27 Å) layer line in the X-ray diffraction pattern (no data from other odd-numbered layer lines were included).

We do not know the reason for these remaining differences. Discrepancies in the central sections of the protofilaments could obviously be due to failure of the negative stain to penetrate fully into this region, even in the case of the zinc–tubulin sheets, which seem to stain better than normal tubulin structures. But this explanation is not adequate for the differences observed in the surface structure. One must postulate that the negative stain does not adequately represent the native protein contours. This might be due to selective positive staining[22] of certain parts of the protein molecules. Alternatively, there may be reproducible changes in conformation during negative staining and dehydration of the EM specimens, as there seems to have been a consistent shrinkage of the sheets. Neither of these possible effects could be corrected for when the negatively stained density distribution was 'stretched' (Fig. 4) to adjust the dimensions to those of hydrated protein. Because of this lack of exact correspondence between the two images, we still cannot be sure that the relative phases, especially those related to features on the inside of the cylinder, are quite correct.

Resolution of the remaining uncertainties in the structure at this resolution must await an independent determination of the Bessel function assignments and phases in the X-ray diffraction pattern, for example, by labelling the protein with heavy atoms[23], if this proves possible. However, the consistency between the results obtained by electron microscopy and X-ray diffraction is clearly much better than it originally seemed to be[5–7] and, for this reason, we believe that the three-dimensional model of zinc–tubulin protofilaments presented here is a good first approximation to the low resolution structure of assembled tubulin.

We thank Drs A. Klug, R. Henderson and P. N. T. Unwin for advice. This work was aided by a grant from the Jane Coffin Childs Memorial Fund for Medical Research. During the course of the work, T.S.B. was a fellow of the Jane Coffin Childs Memorial Fund.

Received 16 February; accepted 8 May 1979.

1. Chasey, D. *Expl Cell Res.* **74,** 140–146 (1972).
2. Erickson, H. P. *J. Cell Biol.* **60,** 153–167 (1974).
3. Amos, L. A. & Klug, A. *J. Cell Sci.* **14,** 523–549 (1974).
4. Crepeau, R. H., McEwen, B., Dykes, G. & Edelstein, S. J. *J. molec. Biol.* **116,** 301–315 (1977).
5. Cohen, C., Harrison, S. C. & Stephens, R. E. *J. molec. Biol.* **59,** 375–380 (1971).
6. Cohen, C., DeRosier, D. J., Harrison, S. C., Stephens, R. E. & Thomas, J. *Ann. N.Y. Acad. Sci.* **253,** 53–59 (1975).
7. Mandelkow, E., Thomas, J. & Cohen, C. *Proc. natn. Acad. Sci. U.S.A.* **74,** 3370–3374 (1977).
8. Larsson, H., Wallin, M. & Edstrom, A. *Expl Cell Res.* **100,** 104–110 (1976).
9. Gaskin, F. & Kress, Y. *J. biol. Chem.* **252,** 6918–6924 (1977).
10. Kirschner, M. W., Williams, R. C., Weingarten, M. & Gerhart, J. C. *Proc. natn. Acad. Sci. U.S.A.* **71,** 1159–1163 (1974).
11. Baker, T. S. & Amos, L. A. *J. molec. Biol.* **123,** 89–106 (1978).
12. Crepeau, R. H., McEwen, B. & Edelstein, S. J. *Proc. natn. Acad. Sci. U.S.A.* **75,** 5006–5010 (1978).
13. Amos, L. A. & Baker, T. S. *Int. J. biol. Macromolec.* (submitted).
14. Henderson, R. & Unwin, P. N. T. *Nature* **257,** 28–32 (1975).
15. Luduena, R. F., Shooter, E. M. & Wilson, L. *J. biol. Chem.* **252,** 7006–7014 (1977).
16. Tilney, L. G. *et al. J. Cell Biol.* **59,** 267–275 (1973).
17. Pierson, G. B., Burton, P. R. & Himes, R. H. *J. Cell Biol.* **76,** 223–228 (1978).
18. Warner, F. D. & Satir, P. *J. Cell Sci.* **12,** 313–326 (1974).
19. Amos, L. A. *J. Cell Biol.* **72,** 642–654 (1977).
20. Amos, L. A. in *Microtubules* (eds Roberts, K. & Hyams, J.S.) (Academic, London, 1979).
21. Unwin, P. N. T. & Henderson, R. *J. molec. Biol.* **94,** 425–440 (1975).
22. Unwin, P. N. T. *J. molec. Biol.* **98,** 235–242 (1975).
23. Holmes, K. C., Stubbs, G. J., Mandelkow, E. & Gallwitz, U. *Nature* **254,** 192–196 (1975).